Ultrasound in Med. & Biol., Vol. 37, No. 12, pp. 2096–2104, 2011

0301-5629/$ - see front matter

ELSEVIER

doi:10.1016/j.ultrasmedbio.2011.08.008

● *Original Contribution*

SIMULTANEOUS BACKSCATTER AND ATTENUATION ESTIMATION USING A LEAST SQUARES METHOD WITH CONSTRAINTS

KIBO NAM,* JAMES A. ZAGZEBSKI,† and TIMOTHY J. HALL†

*Department of Electrical and Computer Engineering, University of Wisconsin-Madison, Madison, WI, USA; and
†Department of Medical Physics, University of Wisconsin-Madison, Madison, WI, USA

(*Received* 21 *February* 2011; *revised* 29 *July* 2011; *in final form* 10 *August* 2011)

Abstract—Backscatter and attenuation variations are essential contrast mechanisms in ultrasound B-mode imaging. Emerging quantitative ultrasound methods extract and display absolute values of these tissue properties. However, in clinical applications, backscatter and attenuation parameters sometimes are not easily measured because of tissues inhomogeneities above the region-of-interest (ROI). We describe a least squares method (LSM) that fits the echo signal power spectra from a ROI to a three-parameter tissue model that simultaneously yields estimates of attenuation losses and backscatter coefficients. To test the method, tissue-mimicking phantoms with backscatter and attenuation contrast as well as uniform phantoms were scanned with linear array transducers on a Siemens S2000. Attenuation and backscatter coefficients estimated by the LSM were compared with those derived using a reference phantom method (Yao et al. 1990). Results show that the LSM yields effective attenuation coefficients for uniform phantoms comparable to values derived using the reference phantom method. For layered phantoms exhibiting nonuniform backscatter, the LSM resulted in smaller attenuation estimation errors than the reference phantom method. Backscatter coefficients derived using the LSM were in excellent agreement with values obtained from laboratory measurements on test samples and with theory. The LSM is more immune to depth-dependent backscatter changes than commonly used reference phantom methods. (E-mail: kibonam@wisc.edu) **© 2011 World Federation for Ultrasound in Medicine & Biology.**

Key Words: **Attenuation, Backscatter, Quantitative ultrasound, Least squares method.**

INTRODUCTION

Pulse-echo ultrasound imaging is a qualitative modality in that image brightness and other features of displayed echo signals depend on operator settings and on system and tissue-dependent factors. In contrast, quantitative ultrasound methods are under development that extracts estimates of attenuation and backscatter on an absolute scale, and other features that depend directly on acoustic wave-tissue interactions. Quantitative ultrasound (QUS) has shown potential for detecting diffuse disease and for diagnosing focal lesions. For example, measurements of ultrasound attenuation were used to differentiate fatty liver from normal liver (Fujii et al.2002; Narayana and Ophir 1983) while other researchers demonstrated that ultrasound attenuation has diagnostic value in trabecular bone (Wear 2003), cortical bone (Sasso 2008) and in the breast (Golub et al. 1993; Huang and Li 2005). Spectral analysis of backscattered echo signals has been used successfully to differentiate benign from malignant masses in the eyes (Liu et al. 2004), lymph nodes (Feleppa et al. 1997; Mamou et al. 2009) and to outline high risk regions to guide prostate biopsies (Feleppa et al. 2000). A scatterer size estimator was successfully applied to backscatter data to accurately estimate glomerular and arteriole sizes in kidneys (Insana et al. 1993). Estimation of the effective scatter size from backscattered echo signal power spectra differentiated rat mammary fibroadenomas from 4T1 mouse carcinomas (Oelze et al. 2004). Finally, preliminary data have been obtained to evaluate its role in areas such as identifying malignant thyroid nodules (Wilson et al. 2006) and liver masses (Liu et al. 2007).

We are applying QUS for *in vivo* breast tumor diagnosis. The challenge for quantitative ultrasound in this application is related to the limited size of many breast masses and to the need to correct spectral data for attenuation along the (often heterogeneous) tissue path between the ultrasound transducer and the region-of-interest

Address correspondence to: Kibo Nam, Ultrasound Research Laboratory, Department of Medical Physics, University of Wisconsin-Madison, 1111 Highland Avenue, Madison, WI 53705 USA. E-mail: kibonam@wisc.edu

(ROI). Attenuation and viscous losses compete with scattering to affect the magnitude of detected echo signals. Furthermore, spatial variations in both properties complicate the use of simple reference techniques, such as the reference phantom method developed by our group (Yao et al. 1990) for accounting for both system dependencies of echo signal data and attenuation along the propagation path. Eliminating system dependencies in the data is desirable in QUS to obtain parameter estimates that are independent of the imaging system and the use of a reference phantom is a popular and easy way to account for these system factors. Although reference phantom methods exhibit high accuracy when the ROI is homogeneous, in most *in vivo* breast cases, these conditions are not met.

To account for attenuation effects over an inhomogeneous pathway, Lu et al. (1995) proposed a dual-spectrum method and measured an "effective attenuation coefficient" of the body wall for backscatter studies in the liver. They assumed the frequency dependence of backscatter in the liver and in a reference phantom used in the method was unchanged over their analysis frequency range. Bigelow et al. (2005) introduced a Gaussian transformation algorithm and a Spectral fit algorithm to estimate both the total attenuation and the effective scatterer size. The technique yielded values of total attenuation to a region of interest that agreed to within 20% for some cases. To date the method has not been evaluated using array transducers.

The purpose of this article is to describe a least squares method to estimate the effective attenuation between the ultrasound transducer and a ROI. The approach uses the power spectrum of radio frequency (RF) echo signals from a ROI within the sample as well as the power spectrum acquired from the same depth in a well characterized reference phantom. The ratio of the spectra is fit to a three-parameter tissue model that quantifies the attenuation and backscatter properties of the media. The least squares method is introduced in detail in the next section.

We also present results of phantom tests of the least squares method. Phantoms with depth varying attenuation and depth varying backscatter levels, as well as ones with uniform attenuation and backscatter, were constructed and studied with this technique.

METHODS AND MATERIALS

Least squares with constraints

The least squares method (LSM) is applied to echo signals from a region of tissue that are acquired following broadband excitation of an ultrasound transducer. Assuming the scattering in soft tissue is weak enough to ignore multiple scattering (Born approximation) and the distance from the transducer to the ROI is greater than the transducer aperture, the power spectrum of the backscattered RF echo signals from the region can be written as (Yao et al. 1990)

$$S(f,z) = G(f)\cdot D(f,z)\cdot A(f,z)\cdot B(f), \tag{1}$$

where f denotes frequency and z represents the depth of the ROI. $S(f,z)$ is the power spectrum of the backscattered echo signal and $G(f)$ represents the combined transducer effects from transmitting and receiving an RF signal. $G(f)$ depends on factors such as the transducer design, pulsing characteristics and receiver gain. $D(f,z)$ accounts for beamforming and diffraction effects, $A(f,z)$ represents the total attenuation through the path from the transducer surface to the depth of interest and $B(f)$is the backscatter coefficient vs. frequency in the ROI.

The cumulative attenuation $A(f,z)$ to depth z is assumed to be spatially homogeneous with respect to the transducer surface. Furthermore, we assume attenuation can be approximated as having a linear frequency dependence and so is modeled as

$$A(f,z) = \exp(-4\alpha f z), \tag{2}$$

where α is an effective attenuation coefficient vs. frequency slope for the propagation path. Similarly, the backscatter coefficient $B(f)$ within the ROI is modeled as

$$B(f) = bf^n, \tag{3}$$

where b is a constant coefficient and n expresses the frequency dependence.

Echo data also are acquired from a reference phantom, whose backscatter and attenuation properties are well characterized, using the same transducer, transmit focus and other equipment settings. Assuming the sound speed in the reference and sample media are the same (diffraction characteristics in these media are the same), the ratio of the echo signal power spectrum from the sample to that from the reference phantom at the same depth can be expressed as,

$$\begin{aligned} RS(f,z) &= \frac{S_s(f,z)}{S_r(f,z)} = \frac{B_s(f)}{B_r(f)}\cdot\frac{A_s(f,z)}{A_r(f,z)} \\ &= \frac{b_s f^{n_s}}{b_r f^{n_r}}\exp\{-4(\alpha_s-\alpha_r)f\cdot z\}, \end{aligned} \tag{4}$$

where the subscripts s and r represent the sample and the reference phantom, respectively.

Taking the natural logarithm of both sides of eqn (4), we get

$$\ln\frac{S_s(f,z)}{S_r(f,z)} = \ln\frac{b_s}{b_r} + (n_s-n_r)\ln f - 4(\alpha_s-\alpha_r)f\cdot z. \tag{5}$$

To simplify eqn (5), we substitute the following terms:

$$\ln\frac{S_s(f,z)}{S_r(f,z)} \equiv X(f,z), \ln\frac{b_s}{b_r} \equiv b,\ n_s - n_r \equiv n,\ \alpha_s - \alpha_r \equiv \alpha \quad (6)$$

Then eqn (5) can be written as

$$X(f,z) = b + n\ln f - 4\alpha f z. \quad (7)$$

To solve for the three unknowns, b,n and α in eqn (7), a least squares fitting process is applied over the band of frequencies contained in the echo signal. That is,

$$\left[\hat{b}, \hat{n}, \hat{\alpha}\right] = \arg \min_{b,n,\alpha} \sum_{i=1}^{K} \left(X(f_i,z) - b - n\ln f_i + 4\alpha f_i z\right)^2, \quad (8)$$

where K is the number of frequency components to be used for the least squares fitting and $\hat{b}, \hat{n}, \hat{\alpha}$ are the estimated parameters for the tissue model. Without loss of generality, eqn (8) may be subjected to constraints to keep the result tenable. That is,

$$b_1 \le b \le b_2,\ \ n_1 \le n \le n_2,\ \ \alpha_1 \le \alpha \le \alpha_2, \quad (9)$$

with the search range of each parameter set according to expected ranges for the tissue or sample media within the ROI.

Realistic bounds easily can be made for the range of backscatter coefficients, attenuation coefficients and frequency dependencies of backscatter allowed for the sample, as discussed below. Once b, n and α are estimated, the backscatter function and effective attenuation of the sample are computed using the known values for the reference phantom and eqn (6).

Uniform phantoms

The least squares method was evaluated first by recording echo signal data for two tissue mimicking phantoms with uniform attenuation and backscatter. One was used as a reference (phantom 1) and the other as the unknown sample (phantom 2). Both phantoms were made with 1–45 micrometer diameter glass bead scatterers randomly distributed in an oil and gelatin emulsion (Madsen et al. 2006). The tops of phantom 1 and phantom 2 are covered with a 25 μm thick Saran^{TM} film (Dow Chemical, Midland, MI, USA) and a plastic coated aluminum foil (made by Gammex Inc., Middleton, WI, USA), respectively.

To establish values for acoustic properties of the reference phantom and to allow estimates of the accuracy of the LSM, speeds of sound, attenuation coefficients and backscatter coefficients were measured on test samples containing the phantom media. These test samples have two parallel transmission windows separated by a known distance. The test samples were made at the same time each phantom was manufactured. Narrow band substitution techniques (Madsen et al. 1986) were used to measure sound speeds and attenuation coefficients within the samples, while a broadband reference reflector method (Chen et al. 1993) was used to measure backscatter coefficients. The latter involves determining the echo signal power spectrum within the sample, determining the spectrum from a smooth planar interface and modeling the 3-dimensional (3-D) beam profile as well as the transmission and reception properties of the transducer-pulser-receiver used in the experiment. The accuracy of the Chen method has been reported previously (Chen et al 1993).

The speed of sound within both phantoms is 1492 m/s, as measured at 2.5 MHz. Dispersion in the tissue mimicking materials is negligible, *i.e.*, typically it has resulted in approximately a 3 m/s increase in sound speed for a 20 MHz frequency elevation (Madsen et al. 2010). The measured attenuation from 2–10 MHz was fit to a line to approximate a linear frequency dependence. Attenuation values for the reference phantom (phantom 1) and the sample (phantom 2) were 0.55 dB/cm-MHz and 0.54 dB/cm-MHz, respectively.

Phantoms with attenuation and backscatter contrast

We also applied the LSM to two tissue mimicking phantoms with spatial variations in backscatter and attenuation to test whether the method is sensitive to variations in backscatter and attenuation along the ultrasound beam paths. Phantom 3 (see Fig. 1a) has three layers with equivalent backscatter coefficients but with the middle layer having a higher attenuation coefficient than the other two layers. Phantom 4 (Fig. 1b) has three layers with nearly the same attenuation but the middle layer has a 6 dB higher backscatter coefficient than the other two layers. Both phantoms consist of water based gel with evaporated milk to control attenuation and nominally mean size of 35 μm diameter glass beads to provide scattering (Madsen et al. 1998). The layered surfaces are bonded together and because the media are nearly identical in density and sound speed reflection losses at the interfaces are negligible.

Speeds of sound, attenuation coefficients and backscatter coefficients for each layer were again measured using test samples manufactured during construction of the phantom. Identical lab techniques were applied as for phantoms 1 and 2 to measure these acoustic properties. Properties of the phantom components are summarized in Table 1.

RF data acquisition and analysis

To evaluate the accuracy of the LSM, phantoms were scanned using a Siemens Acuson S2000 system (Siemens Medical Solutions USA, Inc., Malvern, PA, USA) equipped with a 9L4 (192 elements, 3 rows,

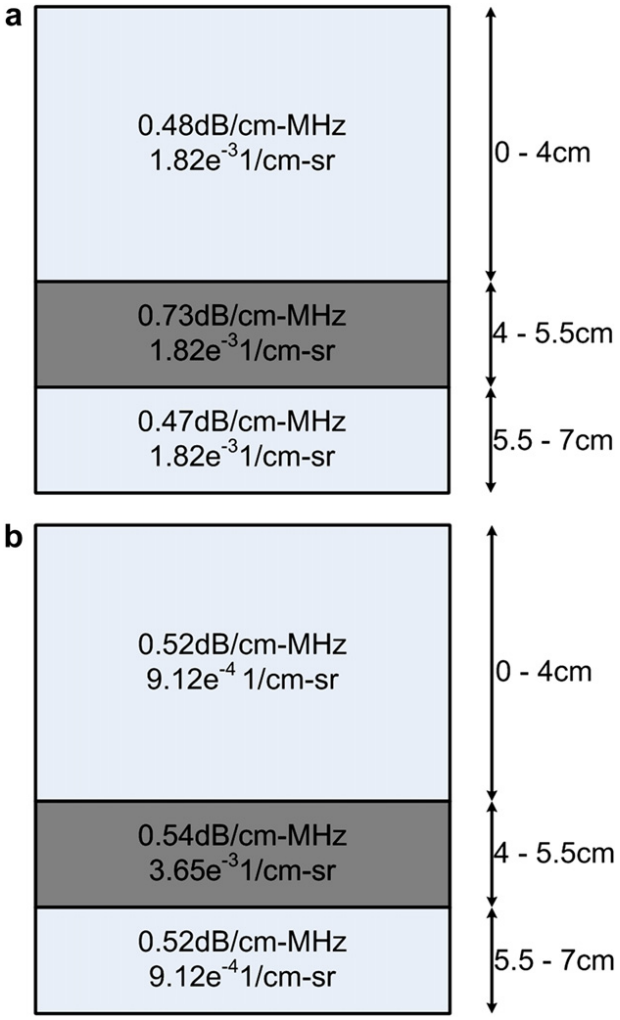

Fig. 1. Layouts of three-layer phantoms (BSC at 7MHz is shown here). (a) Phantom 3: the same BSC throughout but with a higher attenuation in the middle layer. (b) Phantom 4: nearly the same attenuation coefficient throughout, but a higher BSC in the middle layer.

200 micron element pitch) and an 18L6 (576 elements, single row, 100 micron element pitch) linear array transducer. The (nominal) excitation frequencies of the echo data were 9 MHz and 10 MHz for the 9L4 and 18L6 transducers, respectively. The Axius Direct (Brunke et al. 2007) ultrasound research interface on the Siemens system was used to acquire frames of RF data at a 40 MHz sampling frequency. Each frame consisted of 456 and 368 acoustic scan line signals for 9L4 and 18L6 arrays, respectively. This was repeated for seven independent frames, each one acquired after an elevational translation or a rotation of the transducer to obtain statistically independent echo data.

The uniform phantoms and the layered phantoms were scanned at different times and with slightly different equipment settings, *i.e.*, we did not reproduce time-gain compensation and overall gain settings from one experiment to another. However, since RF echo data also were taken from a reference phantom, it was possible to account for any differences in settings on the resulting echo signal spectra. To evaluate the least squares method for uniform paths, phantom 1 was used as a reference and phantom 2 as the sample. With the layered phantoms, where attenuation or backscatter varied along the beam path, each phantom was scanned from the top as seen on the diagrams in Figure 1. In this case "reference phantom" data were taken from the top layer of phantom 3 after rotating it 90 degrees to gain access to this uniform volume.

The echo signal power spectra acquired from ROIs in the phantoms were calculated by applying a Chirp-Z transform (CZT, Rabiner et al. 1969) with a 4 mm long Hann window. Power spectra were evaluated from different regions over a 0.7–6.5 cm (axial) by 0.5–3.3 cm (lateral) area for each frame of echo data. The power spectra analysis windows were overlapped axially by 75%. This was done by incrementing the Hann window 1 mm along the beam path for successive spectral calculations. A single power spectrum was then obtained at each depth by averaging data across acoustic beam lines and from the seven independent planes. For the phantom 2 experiment, the power spectra were corrected by multiplying by the transmission coefficient for the respective scanning windows of the sample and reference phantoms.

Table 1. Properties of layered phantoms

	Top	Middle	Bottom
(a) Phantom 3: Constant backscatter			
Scatterer diameter	5–43 μm	5–43 μm	5–43 μm
Number density	4 g/L	4 g/L	4 g/L
Background material	26% milk, 74% gel	50% milk, 50% gel	26% milk, 74% gel
Speed of sound (at 3.5MHz)	1553 m/s	1564 m/s	1555m/s
Attenuation	0.48 dB/cm-MHz	0.73 dB/cm-MHz	0.47 dB/cm-MHz
(b) Phantom 4: Constant attenuation			
Scatterer diameter	5–43 μm	5–43 μm	5–43 μm
Number density	2 g/L	8 g/L	2 g/L
Background material	3:1 gel to milk	3:1 gel to milk	3:1 gel to milk
Speed of sound (at 3.5MHz)	1552 m/s	1553 m/s	1552m/s
Attenuation	0.52 dB/cm-MHz	0.54 dB/cm-MHz	0.52 dB/cm-MHz

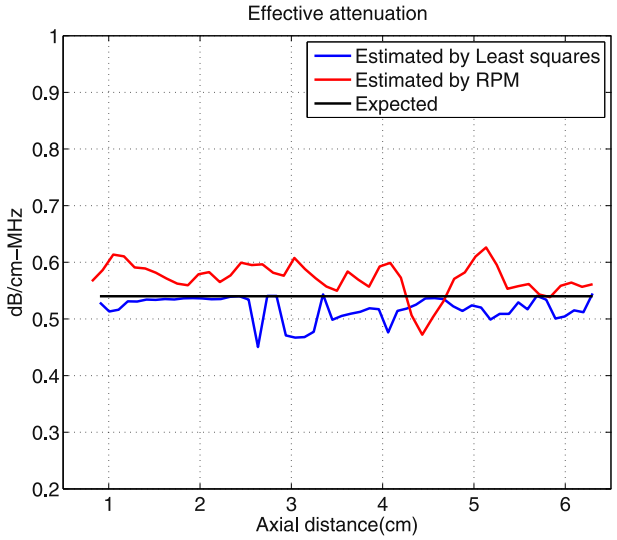

Fig. 2. Effective attenuation coefficients vs. depth results for phantom 2.

With the layered phantoms, the transducer could be placed in direct contact with the tissue-mimicking materials so no transmission corrections were applied as the coupling from transducer-to-phantom was the same in the sample and reference cases.

The constrained least squares method was applied to compute total attenuation to the depth of analysis within the sample as well as the sample's backscatter coefficient at that location. The following constraints were used for phantom 2:

$$10^{-7} \leq b_s \leq 10^{-1},\ 0 \leq n_s \leq 5,\ 0.2 \leq \alpha_s(dB/cm-MHz) \leq 1 \quad (11)$$

The possible attenuation coefficient values included in this analysis extend well beyond the ranges for the reference and sample phantoms involved. For the layered material phantoms, because the attenuation coefficient extended over a broader range than for the homogeneous phantoms, the upper limit of the allowable attenuation coefficient was set to 2 dB/cm-MHz. Other values for the range of fitting parameters were the same as in eqn (11).

Three equations in three unknowns were obtained by differentiating the right side of eqn (8) with respect to each of the three variables and setting the derivatives to 0. These equations were then solved using the least squares method. The frequency range applied in eqn (11) varied with depth so as to include only those frequency components that were at least 20 dB above the noise floor. For shallow depths this extended from 3.7–7 MHz while at the maximum, 6.5 cm depth frequencies from 3.4–5.4 MHz were employed.

For comparison with other methods applied to measure properties of tissues using clinical scanners, attenuation and backscatter coefficients also were measured for the sample phantoms by applying the reference phantom method (Yao et al. 1990) to the same spectral data. As reported by Yao et al. (1990), the log of the ratio of the echo signal power spectra from the sample and reference are plotted as a function of depth and the ratios are fit to straight lines. The slope of this line is proportional to the difference between the attenuation coefficients of the sample and reference phantom. The latter is known so this yields the attenuation coefficient of the sample. Then by substituting measured values and known quantities into eqn (4), the backscatter coefficient of the sample can also be determined.

RESULTS

Effective attenuation coefficients

Effective attenuation coefficient results generated by the least squares method for uniform phantom 2 are shown in Figure 2. The "expected" values are those derived from the laboratory measurements. The reference phantom method (RPM) yields an estimate for the "local" attenuation coefficient centered within 8-mm analysis windows. RPM results were converted to effective attenuation coefficients by summing overlying local attenuation increments to the analysis window and then dividing by the depth of the window. Because phantom 2 is uniform, the effective attenuation coefficient equals the local attenuation coefficient throughout. The estimated attenuation coefficient results from the least squares method and the RPM are in agreement with the expected values to within 16.6%, with an average error of 4.0% and within 16.0% with average error of 6.9%, respectively.

Results for the measured attenuation coefficients in the heterogeneous phantoms are shown in Figures 3 and 4. Here LSM-measured effective attenuation coefficients vs. depth are compared with results obtained using the reference phantom method and with expected values obtained from laboratory measurements on test samples. Note, the values reported in these plots are the total attenuation to the ROI divided by the depth of the ROI and, hence, are given in dB/cm-MHz. Since the transducer was in direct contact with the layered phantom and the path is uniform for the first 4 cm, the expected effective attenuation coefficient over this region is the same as the local attenuation coefficient. Then, beginning at 4 cm, *i.e.*, the depth of the interface between the top and middle layers, there is a gradual increase in the expected and measured effective attenuation coefficient values because of a greater attenuation within the middle layer contributing to the total attenuation to the ROI. In a like manner, the effective attenuation coefficient predictably decreases for points beyond the higher

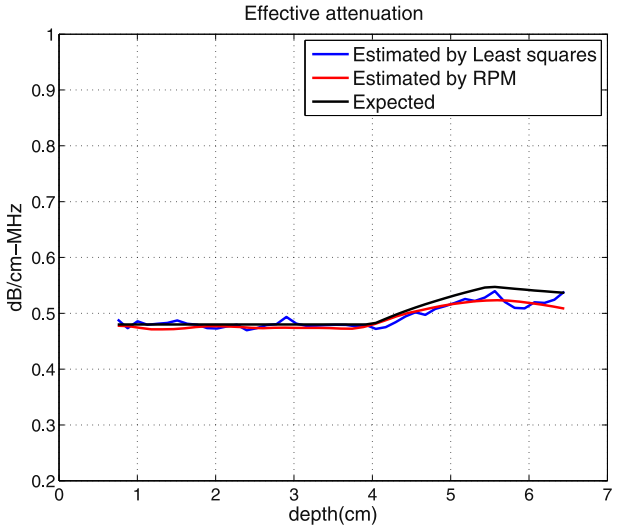

Fig. 3. Effective attenuation coefficients results for phantom 3.

attenuating layer. Results from the RPM were interpreted as effective attenuation coefficients at each depth, as was done previously for phantom 2. Since the local attenuation above the ROI could not be calculated due to low signal to noise ratio, the expected (independently measured) local attenuation value was used for effective attenuation coefficient calculations in the RPM results.

As can be seen in the Figures 3 and 4, the estimated effective attenuation coefficients from the least squares method are in good agreement with the expected values for both phantoms. The percent errors are presented in Table 2.

Higher errors were observed from both methods for phantom 4, in which there is a variation in backscatter along the beam path. The performance of the least

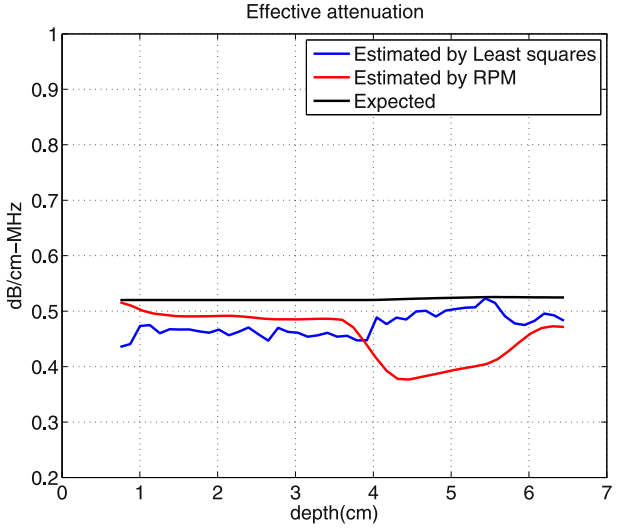

Fig. 4. Effective attenuation coefficients results for phantom 4.

Table 2. Percent errors from effective attenuation coefficients results

	Maximum percent error		Mean percent error	
	Least squares	RPM	Least squares	RPM
Phantom 3	6.3%	5.3%	1.8%	2.0%
Phantom 4	16.2%	27.9%	9.1%	12.5%

RPM = reference phantom method.

squares method was comparable to the RPM results for phantom 3. For phantom 4's results, the least squares method produced an increased bias for the first layer but less bias in the following layers than the reference phantom method. The RPM method used the expected local attenuation value for effective attenuation coefficient calculations and, therefore, had no bias at the start of the ROI. Considering this advantage to the RPM results, the performance of the least squares method for phantoms 3 and 4 was encouraging.

When applying the reference phantom method to the backscattered echo data, large errors in local attenuation estimations occurred at the layer boundaries of phantom 4. The homogeneity of backscatter assumed in the reference phantom method is violated at these interfaces and the effects are vividly displayed in Figure 5 where local attenuation coefficients vs. depth are shown. The high backscatter at the boundary results in an increase in apparent local attenuation at the proximal boundary and a decrease in the local attenuation at the distal boundary, relative to actual attenuation coefficients. The arrows in the figure indicate the boundaries of the layers.

Backscatter coefficients

The results of the simultaneously derived backscatter coefficients for layers within the phantoms are

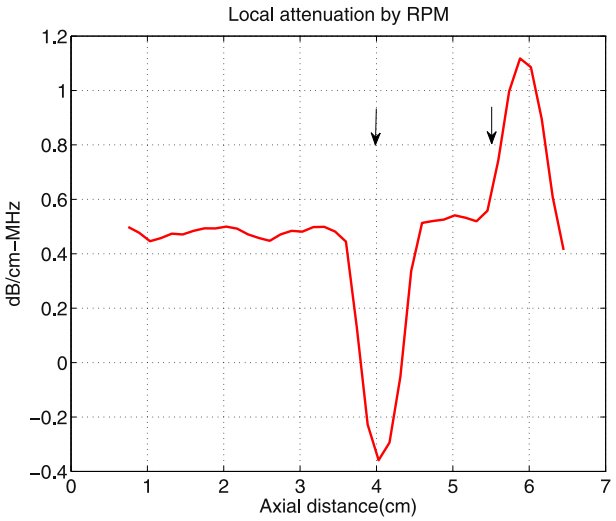

Fig. 5. Local attenuation coefficients by the reference phantom method from phantom 4 (with a high backscatter layer).

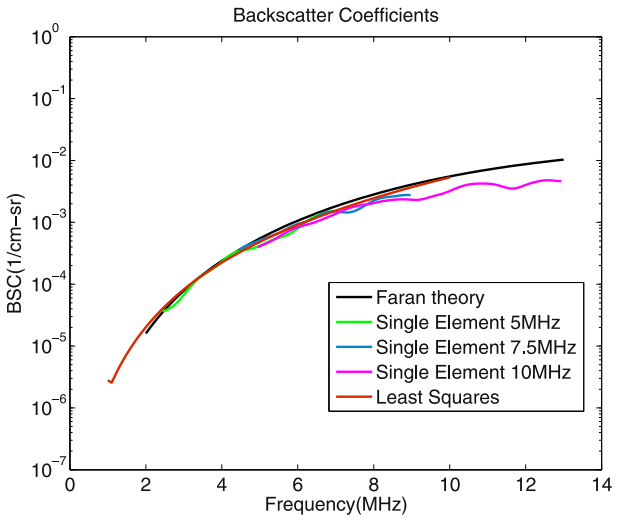

Fig. 6. Comparison of backscatter coefficient measurement for phantom 3.

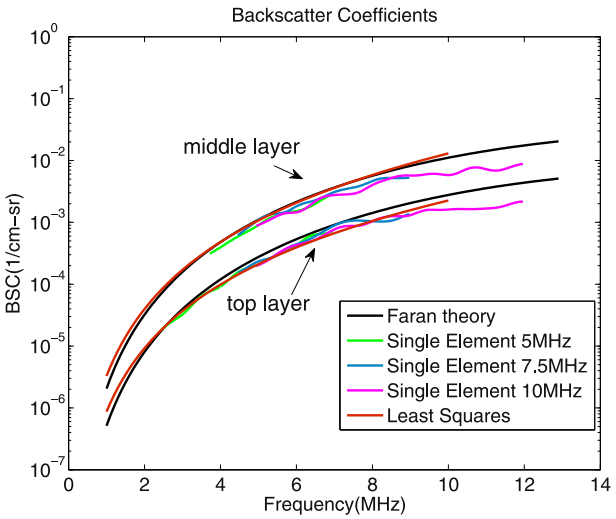

Fig. 7. Comparison of backscatter coefficient measurement for phantom 4.

presented in Figures 6 and 7. These are compared with the established values for the phantom materials that were determined using test samples, as described in the Methods section. Three different single element transducers were used to cover a broad frequency range for the test sample specimens and, hence, three curves are shown for the lab data. Also shown are backscatter coefficients computed by the theory of Faran (1951) using the properties of the glass beads in the phantom, the number density of the beads and their size distribution.

Measured backscatter coefficients obtained with the least squares method are in excellent agreement with results from lab methods and both are in excellent agreement with the values predicted with Faran's theory, though the agreement with the Faran computations was not as good at high frequencies. Such deviations between the measurements and predicted backscatter coefficients are sometimes found when a broad scatterer size distribution is used but too few glass bead scatterer diameters are microscopically measured to adequately predict scattering. We have demonstrated that accurate backscatter coefficient measurements can be made in phantoms with similar broad scatterer size distributions when the added effort is put forth. In this case that effort was deemed unnecessary for this work.

DISCUSSION

Backscatter coefficient determinations for a ROI in tissue require corrections for attenuation losses over the beam path. A least squares method enables these attenuation determinations for cases where the path is acoustically nonuniform. In this article, an effective attenuation coefficient, defined as the total attenuation to the ROI divided by the total path length, is measured by applying the LSM to echo data derived from a clinical scanner equipped with a research interface. Comparisons are made with results obtained from a reference phantom method.

As expected, attenuation coefficients measured using the reference phantom method are in good agreement with actual values when the test sample is uniform and the backscatter coefficient is constant throughout the sample (Phantom 2 results presented in Fig. 2). The reference phantom method resulted in a smaller maximum percent error than the least squares method. However, the least squares method exhibited a lower variance for attenuation measurements within the region of interest, as demonstrated by its lower mean percent error.

Both the reference phantom method and the LSM produced comparable results for phantom 3, in which the backscatter coefficient is the same throughout but the attenuation coefficient along part of the path is significantly elevated (see Fig. 3). However, the reference phantom method resulted in highest errors for phantom 4, in which there was backscatter contrast along the beam path. In this case, the least squares method yielded attenuation results that were within 16% of actual attenuation coefficients for the phantom.

For the nonuniform phantoms used here, the least squares method provided more accurate attenuation and backscatter coefficients than the reference phantom technique. In particular, LSM results were less affected by backscatter variations along the beam propagation path than reference phantom method results, as demonstrated in Figure 4.

For most quantitative techniques, including the LSM, prior knowledge can be applied to help avoid solutions that are physically meaningless, or to enable more rapid

solutions of the estimation problem. In the approach followed in this article we assumed the backscatter coefficient over the ROI can be described by power law frequency dependence, bf^n where f is the frequency in MHz. The range of "allowable" values for n was left very broad. Still the least squares solution converged to the correct value, as demonstrated in Figure 7. Upper bounds on the allowable attenuation coefficient that are beyond general values reported for most soft tissues were applied (2 dB/cm-MHz). Still, the LSM performed well for a phantom whose effective attenuation coefficient is significantly lower than this value. Though we used a broad range of attenuation coefficients and backscatter frequency dependency constraints to test the method, it is likely that for many problems these could be made narrower.

The assumption regarding the attenuation over the field not varying with respect to the transducer aperture appears to be valid for the phantom scanned here, even in the case of the layered phantoms shown in Figure 1. The extent that this assumption breaks down in more complex biologic tissue will be the subject of future studies.

An advantage of the LSM method for assessments of acoustic properties within a ROI is that it only requires calculation of a power spectrum from the depth of interest. This may offer advantages for QUS studies applied to small tumors, for example. If the backscatter coefficients vs. frequency can be approximated as in eqn (3), this method has a significant advantage when estimating backscatter coefficients without prior knowledge of the attenuation along the beam path, as is necessary for "conventional" methods.

One limitation of the least squares method is that it assumes simple functional forms for attenuation and backscatter. If those assumptions are not well met, the measurements from this method may lose accuracy. One solution for this limitation might be applying a piece-wise continuous frequency range. This approach may help to describe the backscatter properties in more detail and will be the subject of future investigations.

Another limitation is the assumption that the sample and reference have the same speed of sound. This algorithm is applied to the ratio of echo signal power spectra derived from a sample and from a reference phantom at the same depth. System and diffraction dependencies on the spectra are effectively eliminated when the ratio is taken, providing that the sample and the reference phantom have the same speed of sounds and when the assumed sound speed in the beam-former of an array system also matches the sound speeds in the media. We are investigating effects on attenuation measurements when there are speeds of sound mismatches among the sample, reference phantom and beam-former as a next step.

CONCLUSION

The least squares method described in this article provides accurate measures of the total attenuation along the beam path as well as the backscatter coefficient vs. frequency in homogeneous as well as in 1-dimensional (1-D) inhomogeneous phantoms.

Acknowledgments—The assistance of Dr. Ernest Madsen and Mr. Gary Frank who constructed the phantoms used in this study is gratefully acknowledged. This work was supported by NIH Grant R01CA111289.

REFERENCES

Bigelow TA, Oelze ML, O'Brien WD. Estimation of total attenuation and scatterer size from backscattered ultrasound waveforms. J Acoust Soc Am 2005;117:1431–1439.

Brunke SS, Insana MF, Dahl JJ, Hansen C, Ashfaq M, Ermert H. An ultrasound research interface for a clinical system. IEEE Trans Ultrason Ferroelectr Freq Control 2007;54:198–210.

Chen JF, Zagzebski JA, Madsen EL. Tests of backscatter coefficient measurement using broadband pulses. IEEE Trans Ultrason Ferroelectr Freq Control 1993;40:603–607.

Faran JJ. Sound scattering by solid cylinders and spheres. J Acoust Soc Am 1951;23:405–418.

Feleppa EJ, Machi J, Noritomi T, Tateishi T, Oishi R, Yanagihara E, Jucha J. Differentiation of metastatic from benign lymph nodes by spectrum analysis *in vitro*. Proc IEEE Ultrason Symp 1997;2:1137–1142.

Feleppa EJ, Urban S, Kalisz A, Lizzi FL, Fair WR, Porter CR. Advanced ultrasonic imaging of the prostate for guiding biopsies and for planning and monitoring therapy. Proc IEEE Ultrason Symp 2000;2:1399–1403.

Fujii Y, Taniguchi N, Itoh K, Shigeta K, Wang Y, Tsao JW, Kumasaki K, Itoh T. A new method for attenuation coefficient measurement in the liver: Comparison with the spectral shift central frequency method. J Ultrasound Med 2002;21:783–788.

Golub RM, Parsons RE, Sigel B, Feleppa EJ, Justin J, Zaren HA, Rorke M, Sokil-Melgar J, Kimitsuki H. Differentiation of breast tumors by ultrasonic tissue characterization. J Ultrasound Med 1993;12:601–608.

Huang SW, Li PC. Ultrasonic computed tomography reconstruction of the attenuation coefficient using a linear array. IEEE Trans Ultrason Ferroelectr Freq Control 2005;52:2011–2022.

Insana MF, Hall TJ, Wood JG, Yan ZY. Renal ultrasound using parametric imaging techniques to detect changes in microstructure and function. Invest Radiol 1993;28:720–725.

Liu T, Lizzi FL, Silverman RH, Kutcher GJ. Ultrasonic tissue characterization using 2-D spectrum analysis and its application in ocular tumor diagnosis. Med Phys 2004;31:1032–1039.

Liu W, Zagzebski JA, Kliewer MA, Varghese T, Hall TJ. Ultrasonic scatterer size estimations in liver tumor differentiation. Med Phys 2007;34:2597.

Lu ZF, Zagzebski JA, Madsen EL, Dong F. A method for estimation an overlying layer correction in quantitative ultrasound imaging. Ultrason Imaging 1995;17:269–290.

Madsen EL, Frank GR, Carson PL, Edmonds PD, Frizzell LA, Herman BA, Kremkau FW, O'Brien WD, Parker KJ, Robinson RA. Inter-laboratory comparison of ultrasonic attenuation and speed measurements. J Ultrasound Med 1986;5:569–576.

Madsen EL, Frank GR, Dong F. Liquid or solid ultrasonically tissue-mimicking materials with very low scatter. Ultrasound Med Biol 1998;24:535–542.

Madsen EL, Hobson MA, Shi H, Varghese T, Frank GR. Stability of heterogeneous elastography phantoms made from dispersions in aqueous gels. Ultrasound Med Biol 2006;32:261–270.

Madsen EL, Frank GR, McCormick MM, Deaner ME, Stiles TA. Anechoic sphere phantoms for estimating 3-D resolution of very high frequency ultrasound scanners. IEEE Trans Ultrason Ferroelectr Freq Control 2010;57:2384–2392.

Mamou J, Coron A, Hata M, Machi J, Yanagihara E, Laugier P, Feleppa EJ. Three-dimensional high-frequency characterization of excised human lymph nodes. Proc IEEE Ultrason Symp 2009; 45–48.

Narayana PA, Ophir J. On the frequency dependence of attenuation in normal and fatty liver. IEEE Trans Son Ultrason 1983;30:379–383.

Oelze ML, O'Brien WD, Blue JP, Zachary JF. Differentiation and characterization of rat mammary fibroadenomas and 4T1 mouse carcinomas using quantitative ultrasound imaging. IEEE Trans Med Imaging 2004;23:764–771.

Rabiber L, Schafer R, Rader C. The chirp z-transform algorithm. IEEE Trans Audio Electroacoust 1969;17:86–92.

Sasso M, Haïat G, Yamato Y, Naili S, Matsukawa M. Dependence of ultrasonic attenuation on bone mass and microstructure in bovine cortical bone. J Biomech 2008;41:347–355.

Wear KA. Characterization of trabecular bone using the backscattered spectral centroid shift. IEEE Trans Ultrason Ferroelectr Freq Control 2003;50:402–407.

Wilson T, Chen Q, Zagzebski JA, Varghese T, VanMiddlesworth L. Initial clinical experience imaging scatterer size and strain in Thyroid nodules. J Ultrasound Med 2006;25:1021–1029.

Yao LX, Zagzebski JA, Madsen EL. Backscatter coefficient measurements using a reference phantom to extract depth-dependent instrumentation factors. Ultrason Imaging 1990;12:58–70.